Supporting Information

Single-molecule quantification of photoredox activities and dynamics at the nanoscale on multi-faceted 2D materials

Shuyang Wu, Jinn-Kye Lee, Mingyu Ma, Jia Xin Chan, Zhengyang Zhang*

School of Chemistry, Chemical Engineering and Biotechnology, Nanyang Technological University, 21 Nanyang Link, Singapore 637371.

Corresponding Author

E-mail: zhang.zy@ntu.edu.sg

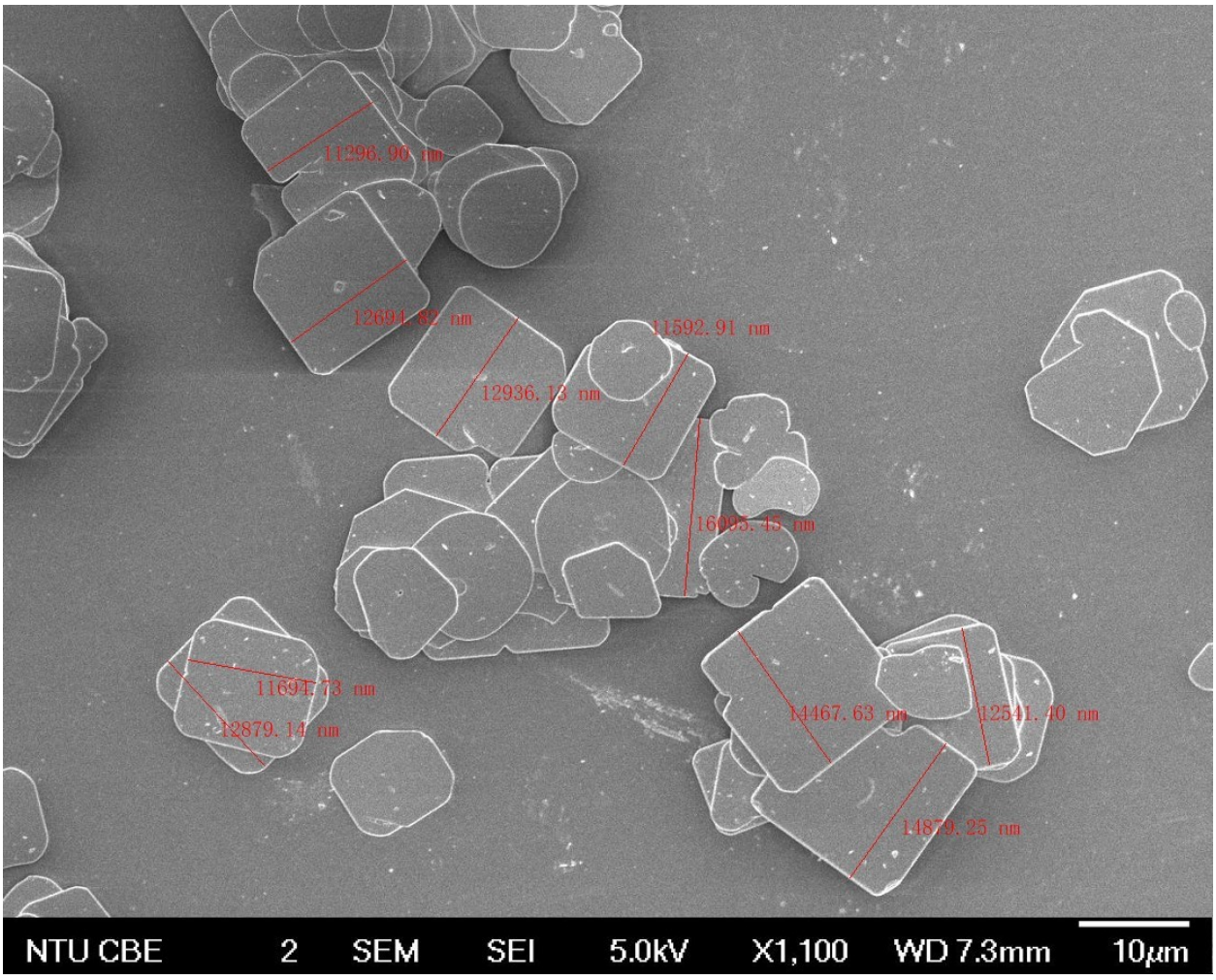

Fig. S1 The FESEM image of BiOBr-001 with lateral size measured.

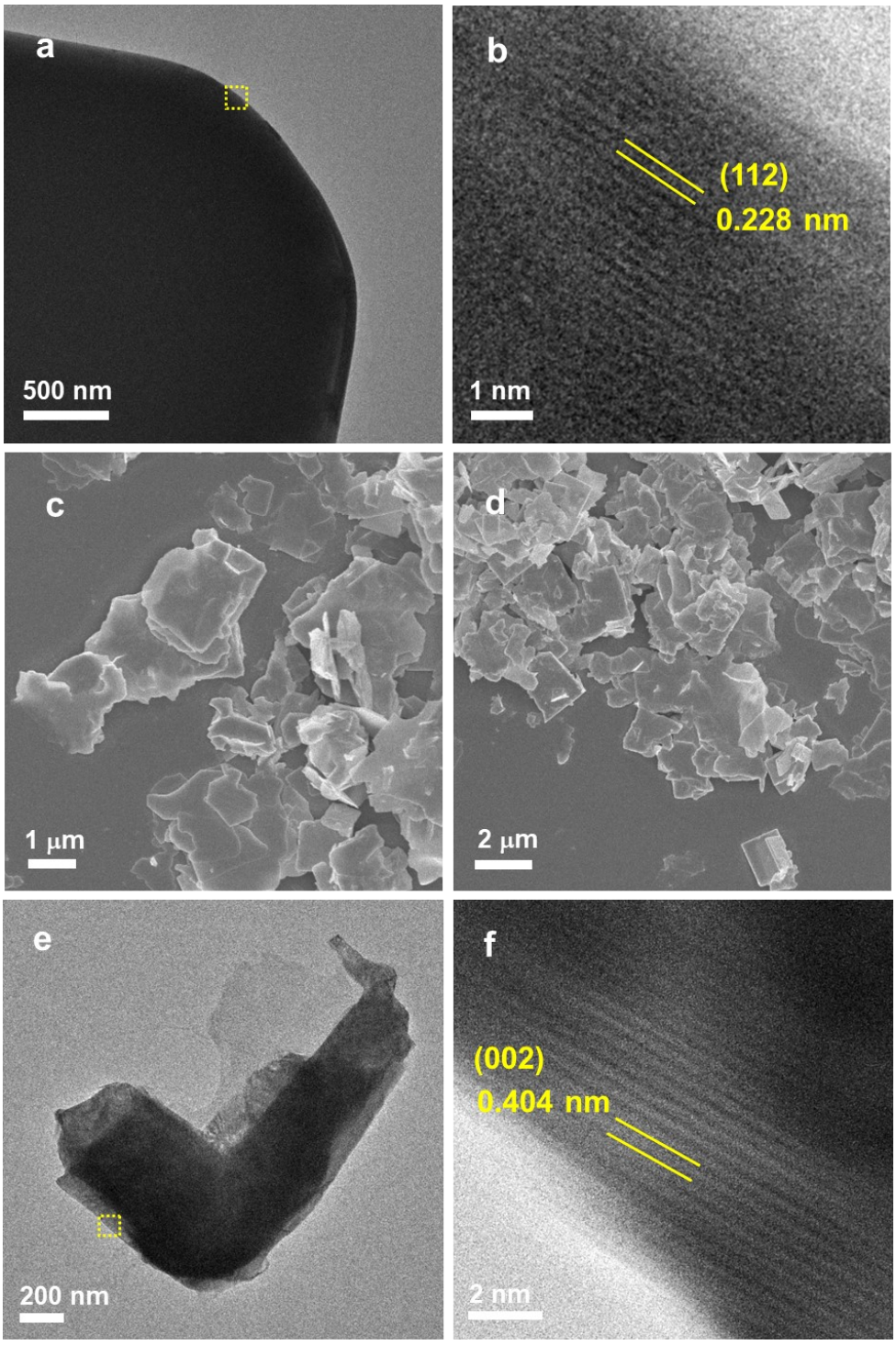

Fig. S2 (a) TEM and (b) HRTEM images of BiOBr-001. (c, d) FESEM, (e) TEM, (f) HRTEM images of BiOBr-010. (b) and (f) are the close-up of the regions in the marked areas in (a) and (e), respectively.

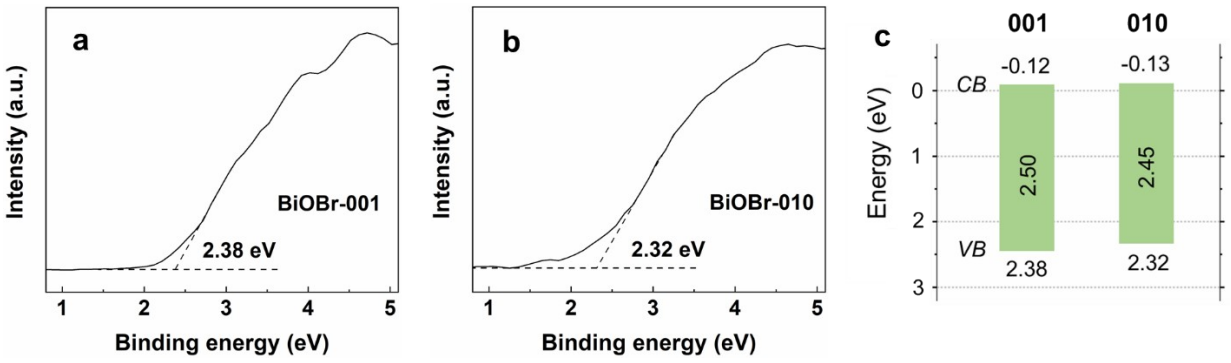

Fig. S3 UPS spectra of (a) BiOBr-001 and (b) BiOBr-010. (c) Band structure diagrams of BiOBr samples.

The principles of SMF imaging of photoredox reactions on BiOBr

To explore charge distribution and photocatalytic heterogeneity at the nanoscale, the SMF technique was employed to visualize the fluorogenic reactions of resazurin photoreduction and amplex red photo-oxidation (**Fig. 2c**). The localization of e^- is achieved through the photoreduction of non-fluorescent resazurin into fluorescent resorufin.[1] The photogenerated h^+ are detected indirectly by oxidizing amplex red to resorufin via hydroxyl radicals (•OH), which are formed through the reaction of h^+ with adsorbed water.[2] As a result, the fluorescence bursts observed in the SMF images represent single catalytic turnover events, where individual fluorescent molecules are produced at distinct catalytic sites (**Fig. 2d**). In the intensity trajectory (**Fig. 2e**), the waiting time before each resorufin molecule forms is denoted as τ_{off}, while τ_{on} represents the time during which resorufin remains at the reactive sites. These events are stochastic single-turnover events, evidenced by the one-step on/off variation in the fluorescence trajectory (**Fig. 2e**). By tracking abundant catalytic events, frames containing single-turnover events are reconstructed and analyzed. In **Fig. S4**, the intensity profile of a resorufin molecule from **Fig. 2d** (highlighted by the cyan square) is depicted as a point spread function spanning multiple pixels. The intensity of the point spread function is fitted to a 2D elliptical Gaussian function, which is used to pinpoint the centers of fluorescent bursts (**Fig. S4**) based on **eqn S1**. According to **eqn S1-S3**, the average localization precision is determined to be 20 nm. The exceptional spatial resolution and high signal-to-noise ratio of the images are attributed to the merits of TIRF microscopy. This imaging method improves photon collection through a high numerical aperture while simultaneously minimizing background noise.

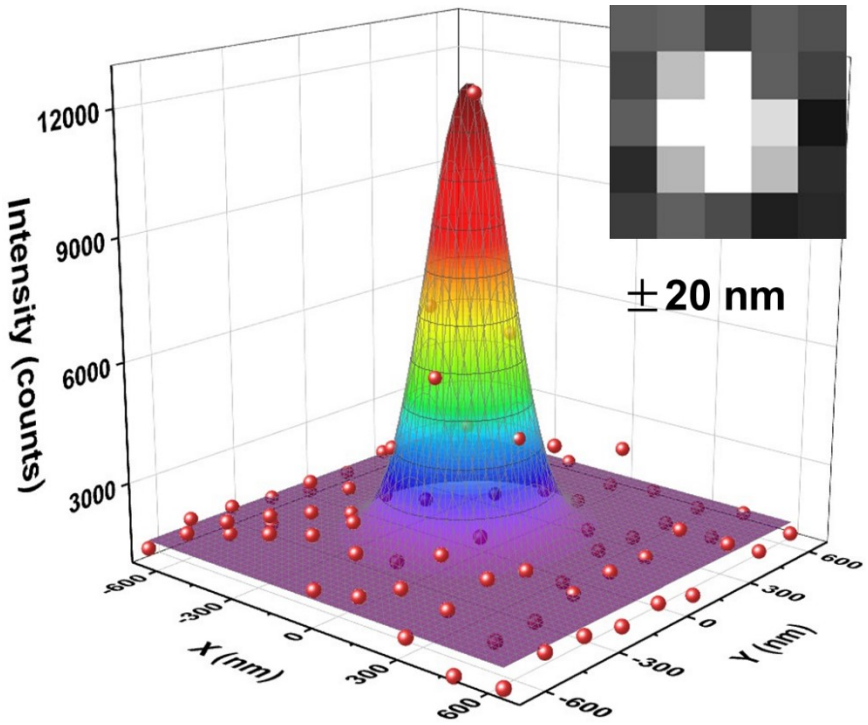

Fig. S4 2D Gaussian fitted distribution of fluorescence intensity of the product molecule in the inset, acquired from the cyan square in **Fig. 2d**.

Determine single-molecule catalytic turnovers with nanometer resolution.

As shown in **Fig. S4**, the fluorescence intensity spreads across several pixels forming a point spread function. In short, the resolution can be calculated using the approach discussed in previous research.[3, 4] **Fig. S4** shows that the center position is determined by fitting the intensity data to 2D elliptical Gaussian functions (**eqn S1**):

$$I(x,y) = A + B * exp(-(\frac{(x-x_0)^2}{2S_x^2} + \frac{(y-y_0)^2}{2S_y^2})) \quad \text{(S1)}$$

where (x_0, y_0) represents the center position, A denotes the background level, B is the peak intensity at (x_0, y_0), S_x and S_y correspond to the standard deviations of the Gaussian distribution along the x- and y-axes, respectively. The localization accuracy ($\sigma_{j,\ j=x,\ y}$) is determined by the pixel size of the camera, the number of photons collected and the background noise level as described in **eqn S2**:

$$\sigma_j = \sqrt{(\frac{S_j^2}{N} + \frac{a^2/12}{N} + \frac{8\pi S_j^4 b^2}{a^2 N^2})} \quad \text{(S2)}$$

where represents the number of photons collected, a is the pixel size, and b denotes the background noise in terms of photons. For the fluorescent burst shown in **Fig. S4**, the parameters are calculated to be S_x = 112 nm, S_y = 120 nm, a = 160 nm, N = 530 and b = 24. As a result, σ_x =19 nm and σ_y =21 nm are determined. The overall localization accuracy (resolution) is calculated to be σ_{xy} = 20 nm using **eqn S3**:

$$\sigma_{xy} = (\sigma_x + \sigma_y)/2 \quad \text{(S3)}$$

Image segmentation.

To quantify the structure-dependent photoactivities and dynamics, image segmentation was performed to define the size of the reaction subregions at each structure (**Fig. S5** and **S6**). Typically, the dimension of the reaction unit area can be determined by analyzing the intensity-position profile.[3] As highlighted by the marked rectangle in **Fig. S5a**, **Fig. S5b** shows the cross-sectional profile of the BiOBr-001 nanoplate when using resazurin. The profile is fitted with a Gaussian function to determine the full width at half maximum (FWHM). The FWHM for BiOBr-001 with resazurin and amplex red is calculated to be 157 nm and 180 nm, respectively (**Fig. S5b,d**). Similarly, the BiOBr-010 sample with resazurin and amplex red shows FWHM values of 156 nm and 164 nm, respectively (**Fig. S6b,d**). These values are approximately the size of one pixel (160 nm). Consequently, the BiOBr samples were divided into multiple subregions of 1 × 1 pixels (160 nm × 160 nm). We ensured that each subregion contained only one fluorescent burst; otherwise, the subregion size is reduced to meet this criterion.

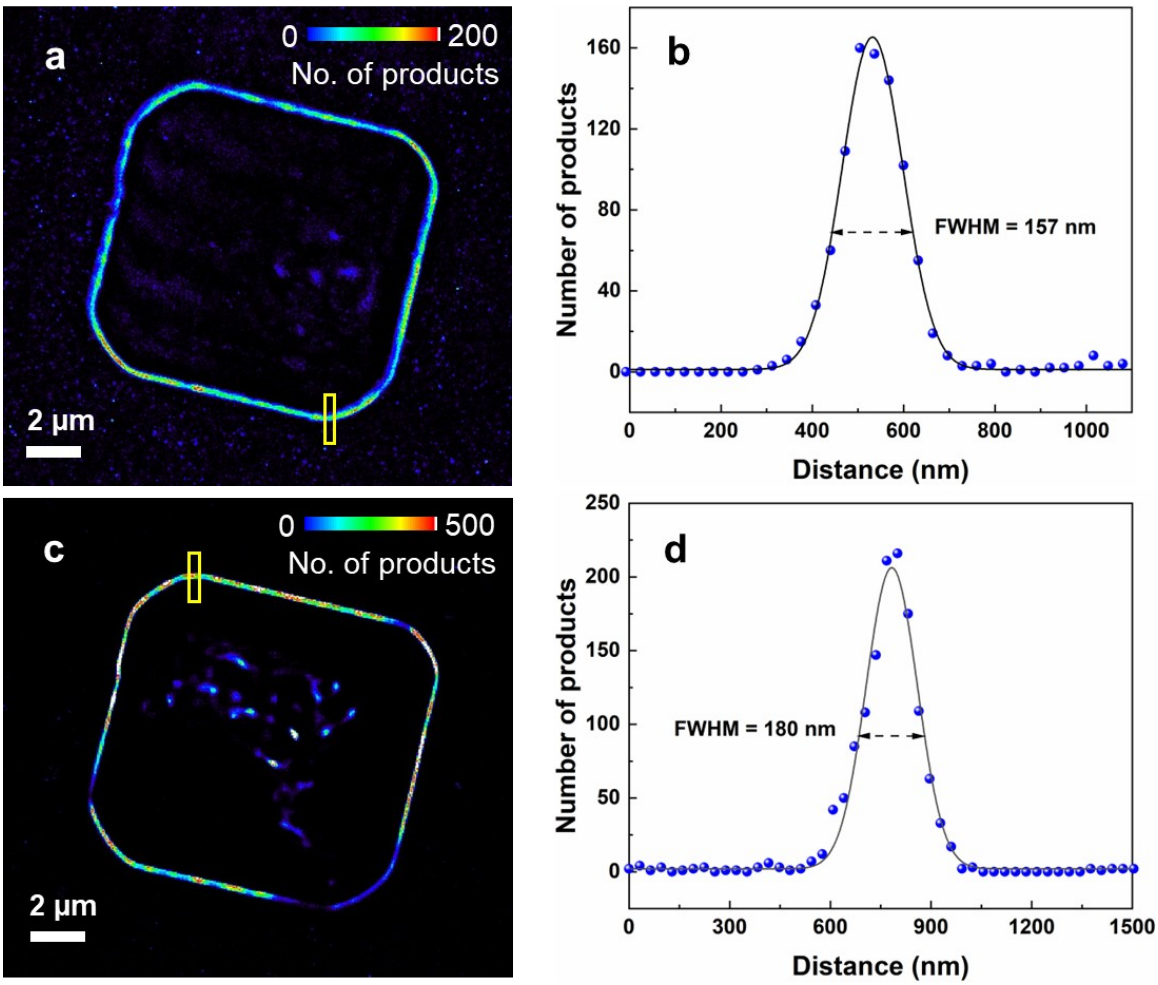

Fig. S5 Image segmentation of BiOBr-001 for (a) resazurin photoreduction and (c) amplex red photo-oxidation in the density map. (b, d) Cross-profile plots of fluorescence intensity on BiOBr-001 marked in (a) and (c), respectively.

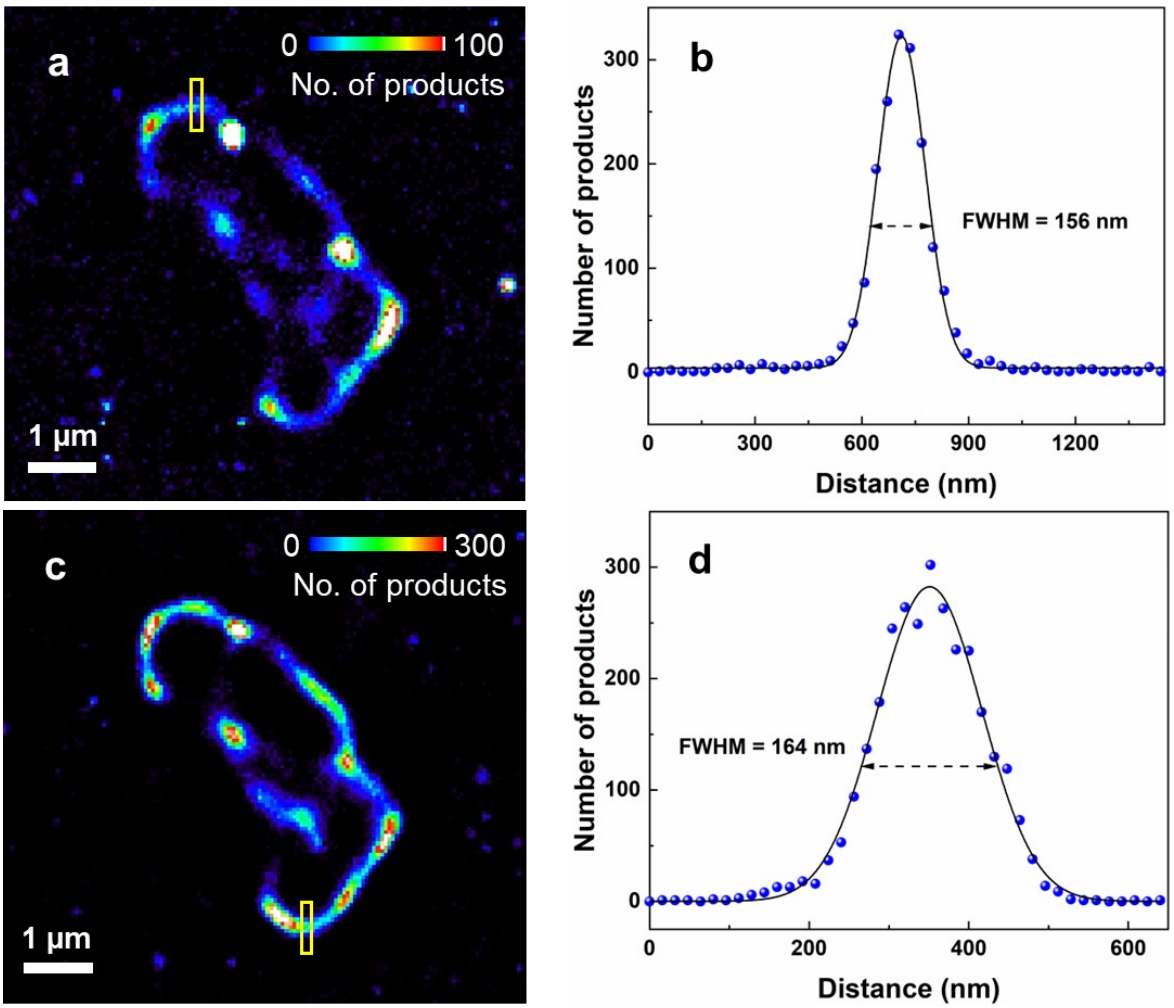

Fig. S6 Image segmentation of BiOBr-010 for (a) resazurin photoreduction and (c) amplex red photo-oxidation in the density map. (b, d) Cross-profile plots of fluorescence intensity on BiOBr-010 marked in (a) and (c), respectively.

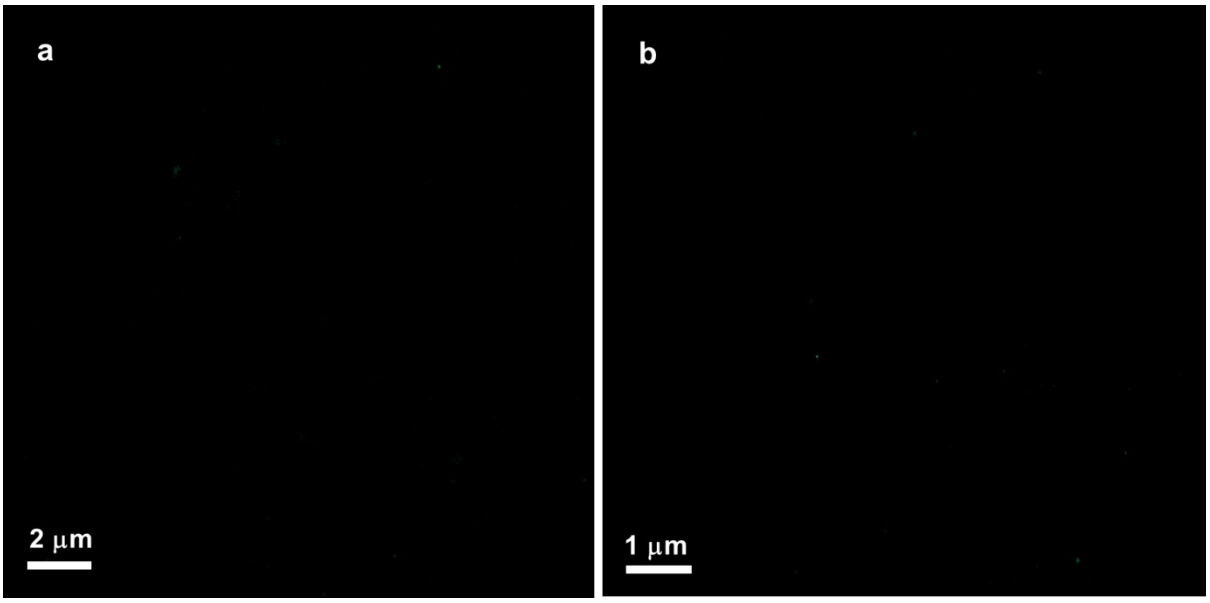

92

93 **Fig. S7** The SMF images of (a) BiOBr-001 and (b) BiOBr-010 after being washed with DI water

94 and photobleached for 30 min after the photoreaction.

95

96

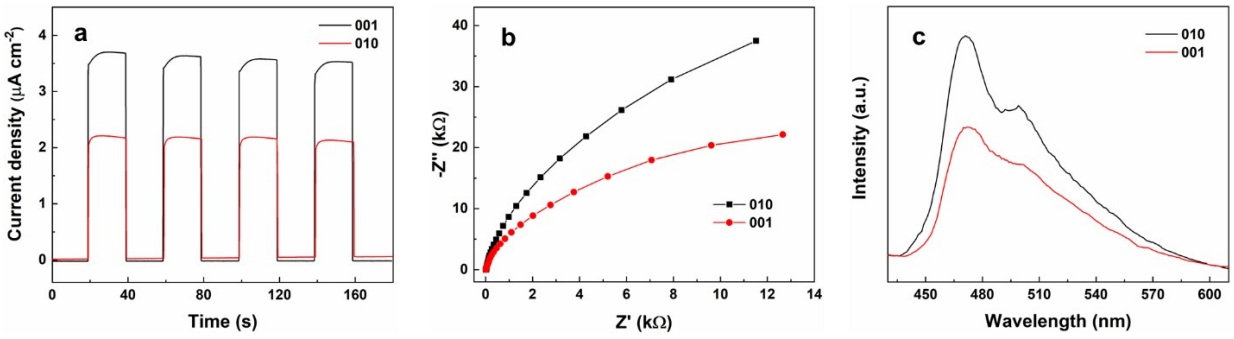

97

98 **Fig. S8** (a) Transient photocurrent density, (b) EIS spectra (300 W Xe lamp, > 400 nm) and (c) PL

99 spectra of BiOBr nanoplates.

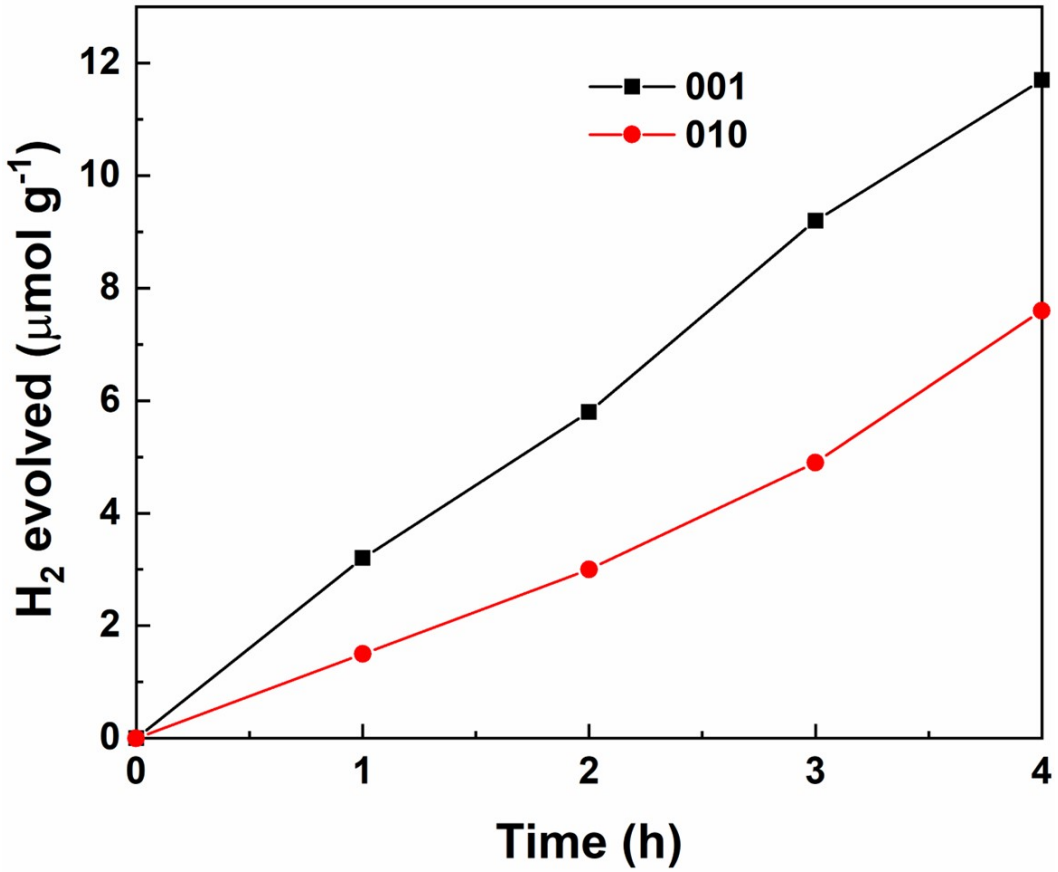

100

101 **Fig. S9** Photocatalytic H_2 generation on BiOBr nanoplates (100 mg of photocatalysts, no Pt

102 cocatalysts, 10 vol% TEOA, 300 W Xe lamp, > 400 nm).

The SMF study of temporal activity fluctuations on BiOBr.

The calculated decay constants for $C_{\tau_{off}}$- m (**Fig. S11a**) and $C_{\tau_{on}}$- m (**Fig. S11b**) are determined to be $m_{off} = 0.81$ and $m_{on} = 1.41$ turnovers, with an average turnover time of 0.33 s for this trajectory. Accordingly, the fluctuation correlation times for τ_{off} and τ_{on} reactions are determined to be 0.27 s and 0.47 s, respectively. These correlation times reflect the fluctuation timescales in the catalytic reaction and indirect product dissociation, which are predominant at the saturated [S] (1 μM). Temporal fluctuations in activity are linked to small-scale dynamic surface restructuring at the nanoscale. This could change the conversion rate constant ($k_{eff} = kn_T$) by altering the reactivity at individual catalytic sites and the number of active sites for τ_{off} reactions. Similarly, it also changes the rate constants of direct and indirect dissociation for τ_{on} reactions. Both will result in temporal variations in activity and oscillatory dynamics. This behavior is driven by distinct adsorbate-surface interactions at each site, which are influenced by [S].[5]

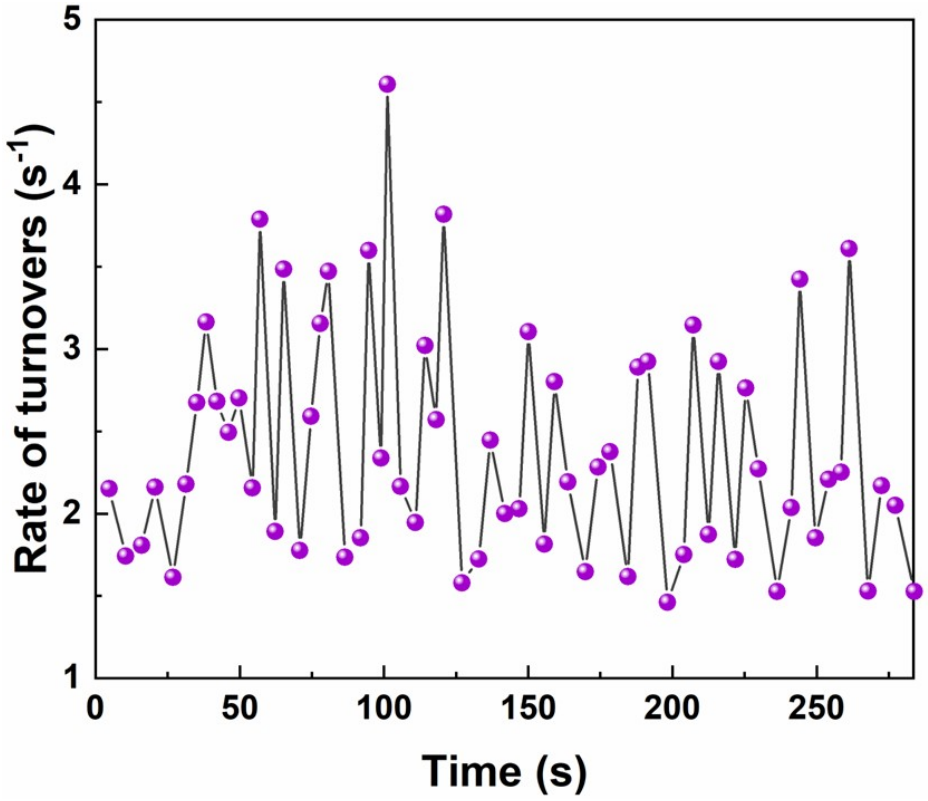

Fig. S10 A typical trajectory of rate of turnovers on BiOBr-001 edges with 1 μM resazurin. Each data point is calculated based on every 10 turnovers.

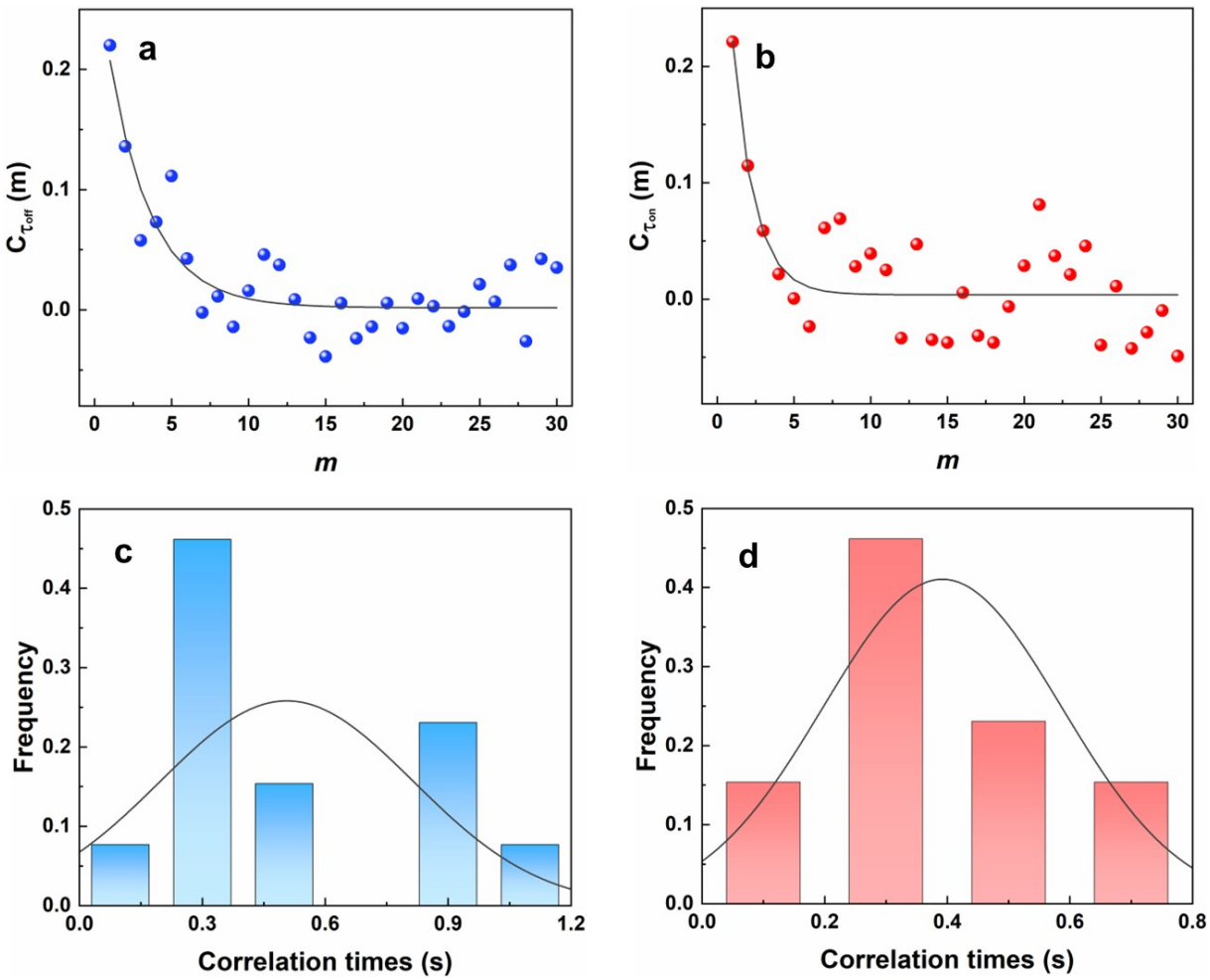

120

121 **Fig. S11** Autocorrelation functions of (a) τ_{off} and (b) τ_{on} reactions from the single-turnover

122 trajectory in **Fig. S10**. Histograms of correlation times of (c) τ_{off} and (d) τ_{on} reactions calculated

123 from numerous subregions (> 10).

124

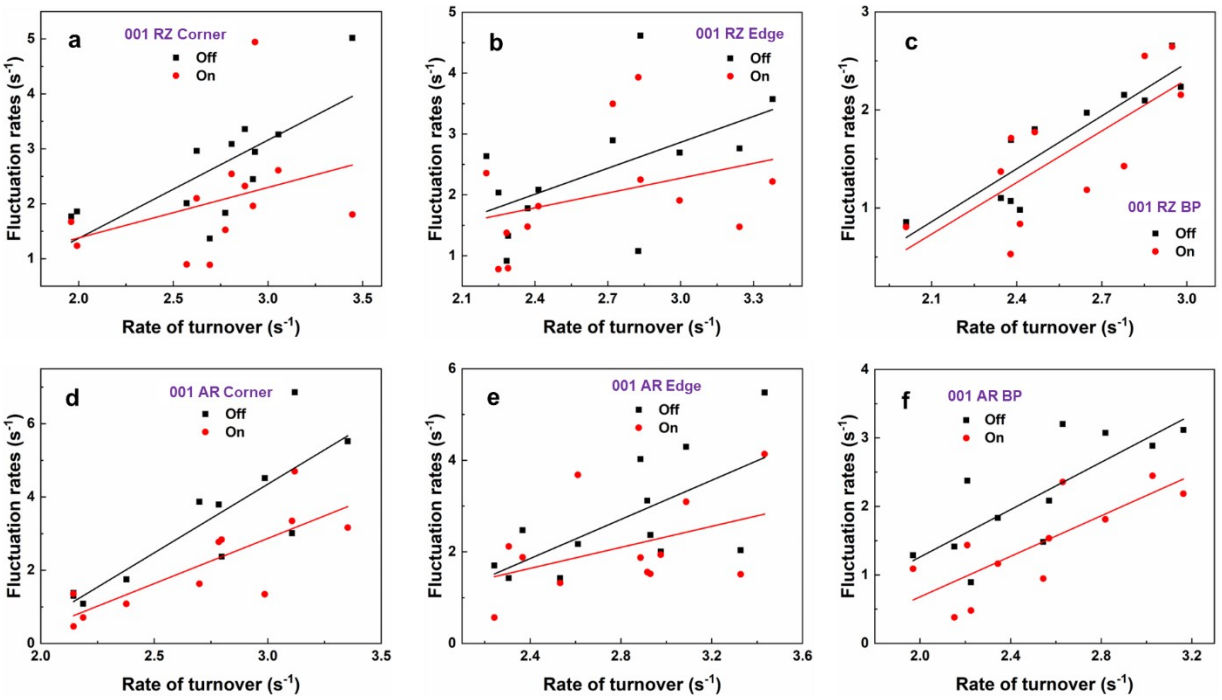

125

126 **Fig. S12** Dependence of photoreduction and photo-oxidation fluctuation rates on rate of turnovers

127 on (a,d) corners, (b,e) edges and (c,f) BPs of BiOBr-001.

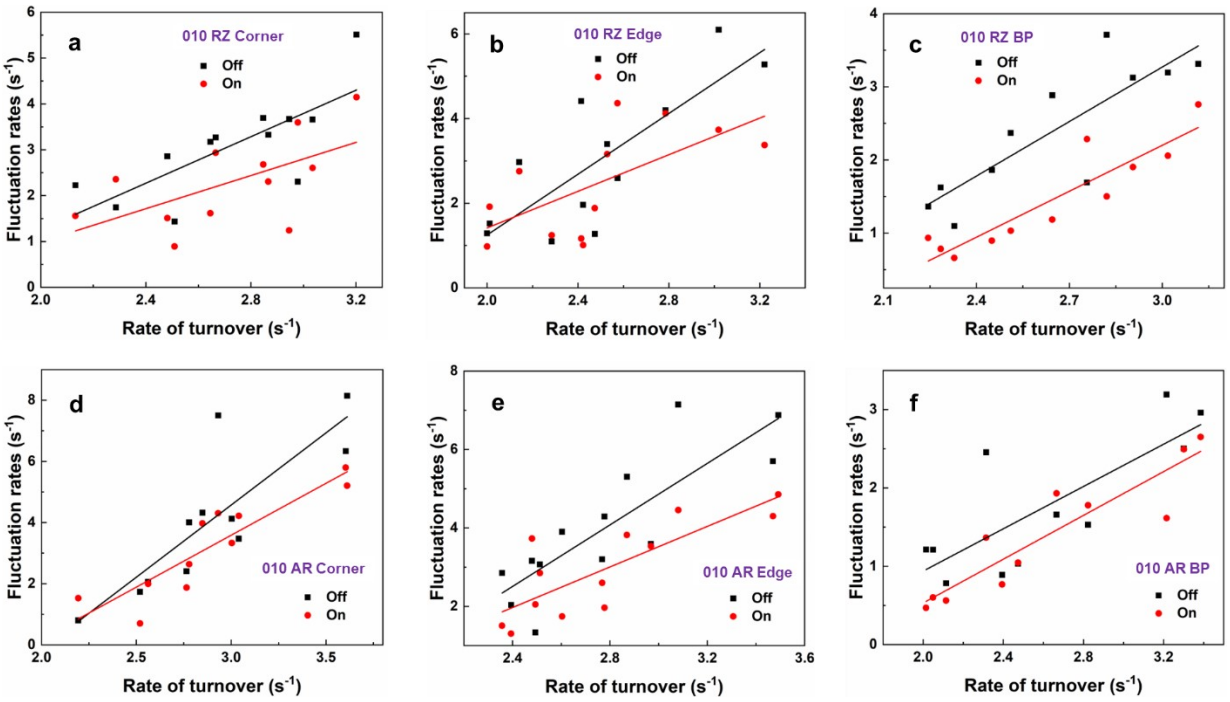

128

129 **Fig. S13** Dependence of photoreduction and photo-oxidation fluctuation rates on rate of turnovers

130 on (a,d) corners, (b,e) edges and (c,f) BPs of BiOBr-010.

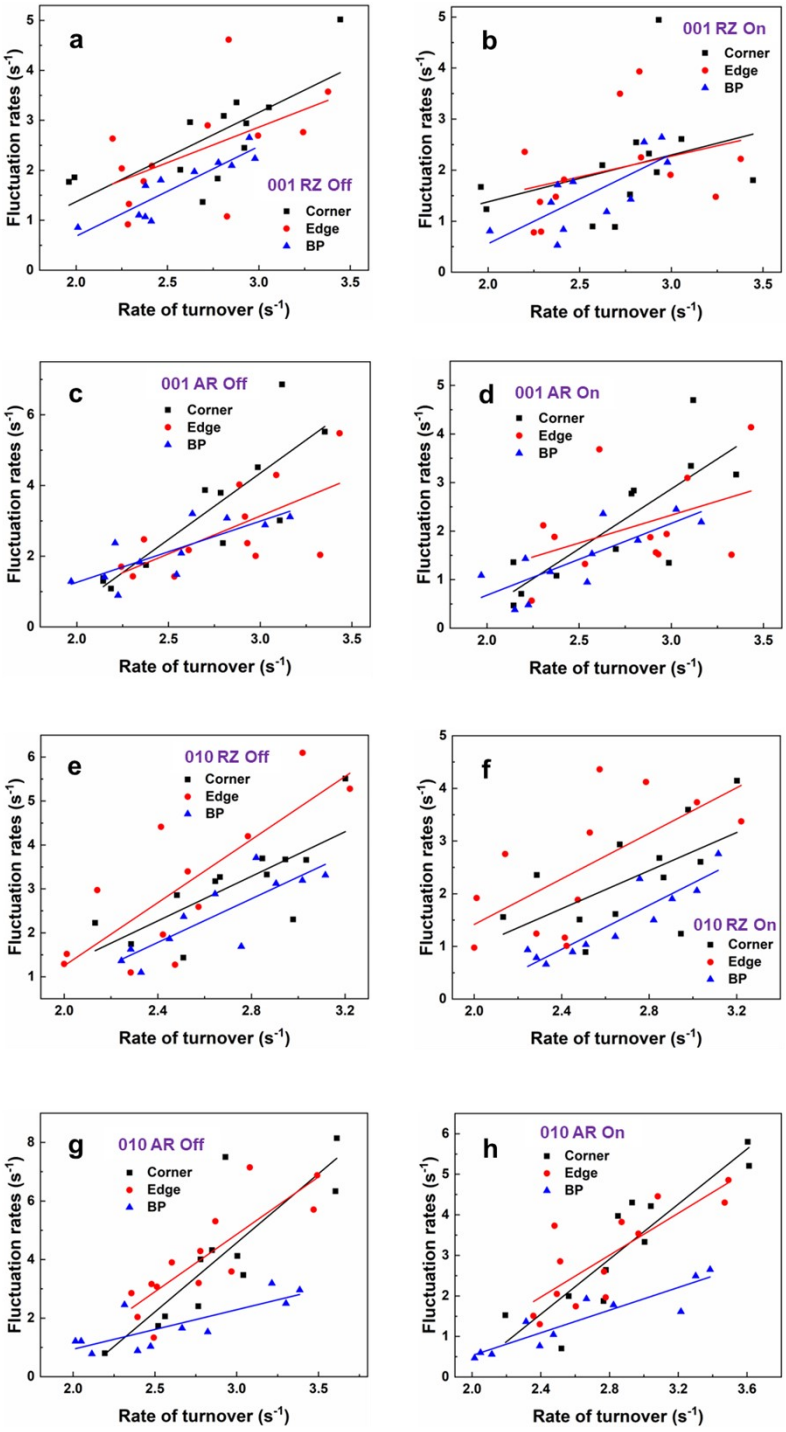

131

132 **Fig. S14** Dependence of τ_{off} and τ_{on} fluctuation rates on rate of turnovers for photoreduction
133 reactions on (a,b) BiOBr-001 and (e,f) BiOBr-010, and photo-oxidation reactions on (c,d) BiOBr-
134 001 and (g, h) BiOBr-010.

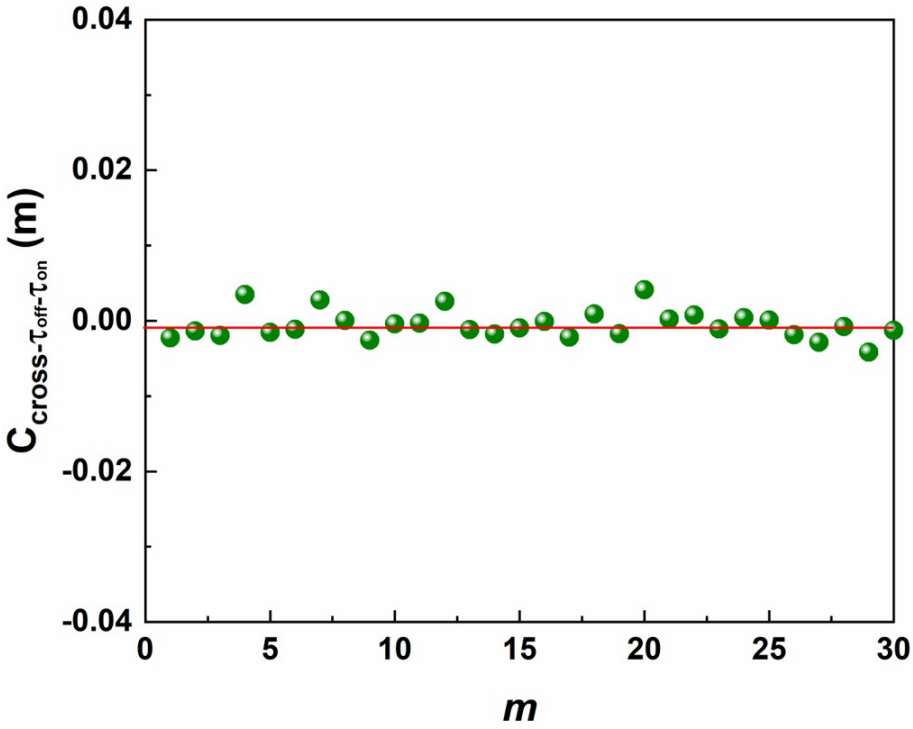

135

136 **Fig. S15** Cross correlation function of τ_{off} and τ_{on} obtained from the trajectory in **Fig. S10**.

137

138

Table S1. Quantification of photoreduction and photo-oxidation activities on corners, edges and BPs of BiOBr nanoplates.

Positions	Photoreduction activity (s^{-1} μm^{-2})	Photo-oxidation activity (s^{-1} μm^{-2})
001-Corner	108.0 ± 11.5	654.5 ± 83.2
001-Edge	84.2 ± 10.0	480.6 ± 63.5
001-BP	3.4 ± 0.7	61.1 ± 12.0
010-Corner	93.3 ± 18.0	191.3 ± 35.3
010-Edge	17.3 ± 3.7	88.3 ± 19.4
010-BP	3.0 ± 0.4	4.7 ± 0.8

Reference

1. M. Shen, T. Ding, W. H. Rackers, C. Tan, K. Mahmood, M. D. Lew and B. Sadtler, *J. Am. Chem. Soc.*, 2021, **143**, 11393-11403.
2. J. W. Ha, T. P. A. Ruberu, R. Han, B. Dong, J. Vela and N. Fang, *J. Am. Chem. Soc.*, 2014, **136**, 1398-1408.
3. T.-X. Huang, B. Dong, S. L. Filbrun, A. A. Okmi, X. Cheng, M. Yang, N. Mansour, S. Lei and N. Fang, *Sci. Adv.*, 2021, **7**, eabj4452.
4. B. Dong, Y. Pei, F. Zhao, T. W. Goh, Z. Qi, C. Xiao, K. Chen, W. Huang and N. Fang, *Nat. Catal.*, 2018, **1**, 135-140.
5. X. Zhou, W. Xu, G. Liu, D. Panda and P. Chen, *J. Am. Chem. Soc.*, 2010, **132**, 138-146.